



HAL
open science

Variability of the temporal bone surface's topography: implications for otologic surgery

Jérémy Lecoœur, Jack H. Noble, Ramya Balachandran, Robert F. Labadie,
Benoit M. Dawant

► To cite this version:

Jérémy Lecoœur, Jack H. Noble, Ramya Balachandran, Robert F. Labadie, Benoit M. Dawant. Variability of the temporal bone surface's topography: implications for otologic surgery. SPIE Medical Imaging 2012, Feb 2012, San Diego, United States. pp.8316-46. hal-00669030

HAL Id: hal-00669030

<https://hal.science/hal-00669030>

Submitted on 15 Feb 2012

HAL is a multi-disciplinary open access archive for the deposit and dissemination of scientific research documents, whether they are published or not. The documents may come from teaching and research institutions in France or abroad, or from public or private research centers.

L'archive ouverte pluridisciplinaire **HAL**, est destinée au dépôt et à la diffusion de documents scientifiques de niveau recherche, publiés ou non, émanant des établissements d'enseignement et de recherche français ou étrangers, des laboratoires publics ou privés.

Variability of the temporal bone surface's topography: implications for otologic surgery

Jérémy Lecoœur^a, Jack H. Noble^a, Ramya Balachandran^b, Robert F. Labadie^b, Benoit M. Dawant^a

^aDepartment of Electrical Engineering and Computer Science, Vanderbilt University, Nashville, TN 37235, USA

^bDepartment of Otolaryngology, Vanderbilt University Medical Center, Nashville, TN 37232, USA

ABSTRACT

Otologic surgery is performed for a variety of reasons including treatment of recurrent ear infections, alleviation of dizziness, and restoration of hearing loss. A typical ear surgery consists of a tympanomastoidectomy in which both the middle ear is explored via a tympanic membrane flap and the bone behind the ear is removed via mastoidectomy to treat disease and/or provide additional access. The mastoid dissection is performed using a high-speed drill to excavate bone based on a pre-operative CT scan. Intraoperatively, the surface of the mastoid component of the temporal bone provides visual feedback allowing the surgeon to guide their dissection. Dissection begins in “safe areas” which, based on surface topography, are believed to be correlated with greatest distance from surface to vital anatomy thus decreasing the chance of injury to the brain, large blood vessels (e.g. the internal jugular vein and internal carotid artery), the inner ear, and the facial nerve. “Safe areas” have been identified based on surgical experience with no identifiable studies showing correlation of the surface with subsurface anatomy. The purpose of our study was to investigate whether such a correlation exists. Through a three-step registration process, we defined a correspondence between each of twenty five clinically-applicable temporal bone CT scans of patients and an atlas and explored displacement and angular differences of surface topography and depth of critical structures from the surface of the skull. The results of this study reflect current knowledge of osteogenesis and anatomy. Based on two features (distance and angular difference), two regions (suprahelical and posterior) of the temporal bone show the least variability between surface and subsurface anatomy.

Keywords: temporal bone, bone topography, otologic surgery, robotic surgery, universal stereotactic frame.

1. DESCRIPTION OF PURPOSE

A large component of otologic surgery involves drilling away a portion of the temporal bone via a procedure known as a mastoidectomy. This operation is similar to an archeological dig where overlying bone is excavated and vital subsurface structures are intended to be identified without damage. In otologic surgery, these structures include the brain, large blood vessels (e.g. the intracranial continuation of the internal jugular vein), nerves (e.g. the facial nerve which controls movement of the face) and the inner ear. During surgical training, surgeons are taught to begin a mastoidectomy in the middle of surface landmarks. The superior surface landmark is a boney ridge that is the continuation of the zygomatic arch (a.k.a. cheekbone) called the temporal line which lies roughly perpendicular to the superior aspect of the root of the ear. A more practical approximation is the posterior projection of straight temple eyeglass pieces. The anterior surface landmark is the most superficial aspect of the external auditory canal. The posterior landmark is considered most variable and consists of a hole in the bone through which a blood vessel called the emissary vein courses. The mid-region of this triangle, called Macewen's triangle^{1,2} (Figure 1), is anecdotally considered to be the safest location to begin surgical intervention. We sought to substantiate this anecdotal finding as future otological surgical techniques, particularly image-guided, minimally-invasive approaches, may have higher dependence on the reliability of surface topography.

One such intervention where this analysis of temporal bone surface topography would be useful is cochlear implantation, a surgery in which hearing loss is treated by inserting an electrode array into the cochlea. Traditional cochlear implantation procedures require wide excavation of the mastoid region of the temporal bone³ to allow surgeons to visualize the critical subsurface structures. Over the last several years, we have developed a less-invasive, image-guided cochlear implantation procedure referred to as percutaneous cochlear implantation (PCI)⁴. In PCI, access to the cochlea is achieved by drilling via a linear path from the surface of the skull through the facial recess to the cochlea. Along the path is the facial recess region that is about 2.4 mm wide and is bounded by the facial nerve, which if damaged causes ipsilateral facial paralysis, and the chorda tympani, which if damaged causes ipsilateral loss of taste sensitivity. To achieve PCI accurately without damage to vital structures, mainly the facial nerve, we employ image-guided surgical (IGS) technology and use three bone-implanted anchors as fiducial markers and a customized microstereotactic frame

that mounts on these anchors and constrains a drill along the desired path. The desired path is computed to be probabilistically safe with respect to sensitive structures⁵, which are segmented using automated techniques we have developed^{6,7,8}

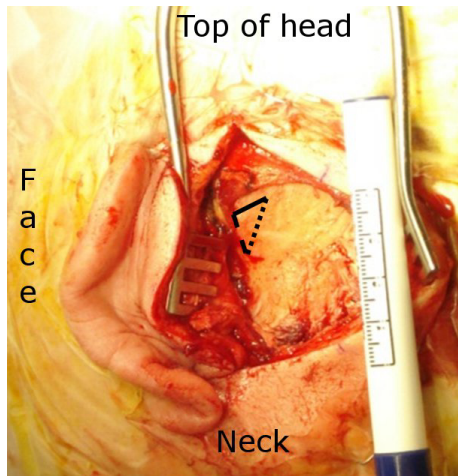


Figure 1 – Macewen’s Triangle for a left ear of a patient is indicated by the region bounded by the three lines—temporal line (solid line), posterior edge of the external auditory canal (dashed line), and the line that connects the other two lines (dotted line).

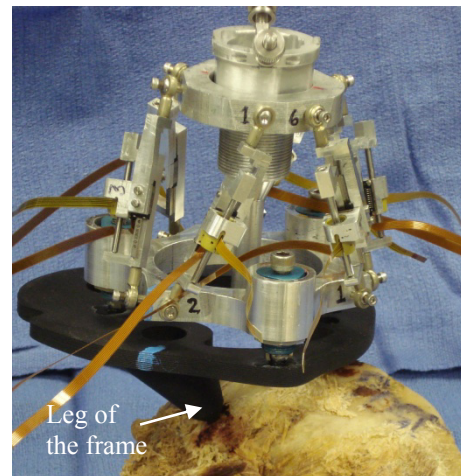


Figure 2 – Prototype of a PCI robot with its fixed frame (black part) mounted on a temporal bone. The frame is rigidly attached to the bone using anchors.

The three bone-implanted fiducial anchors are commonly configured with one in the mastoid tip region, one in the suprahelical region, and one in a posterior region. Through our experience with PCI, we identified that it is necessary to attach the anchors at particular locations in these regions in order to design a suitable microstereotactic frame to achieve the desired trajectory. Currently we are in the process of designing a bone-attached robot⁹ for the drilling task (a prototype of the robot is visible on Figure 2). For this robot, we need to define a universal frame for mounting the robot easily on every patient. Such a fixed robotic frame calls for fixed angle of each leg of the frame with respect to the surface of the bone to enable rigid attachment of the frame and robot to the bone and for fixed lengths between the anchor points. To define the locations of the anchors onto which the fixed robot frame will be mounted, we designed this study to explore the variability of the surface of the temporal bone region around the ear canal in order to find the least varying areas in both displacement and angle amongst the patients.

2. METHODS

2.1. Images

Clinically-applicable temporal bone CT scans of twenty five patients were used in this study with various field of view, resolution, quality, and orientation. A typical scan is $768 \times 768 \times 205$ voxels with, approximately, $0.215 \times 0.215 \times 0.336$ mm³ voxel size. Another CT scan was used as the reference (atlas) volume. This scan is $768 \times 768 \times 145$ voxels with $0.21875 \times 0.21875 \times 0.4$ mm³ voxel size.

2.2. Registration procedure

The temporal bone of each patient was registered to the atlas using a three-step process. (1) The patient CT and the atlas were rigidly registered globally using an intensity-based registration algorithm based on normalized mutual information¹⁰. Figure 3 shows the result of this registration.

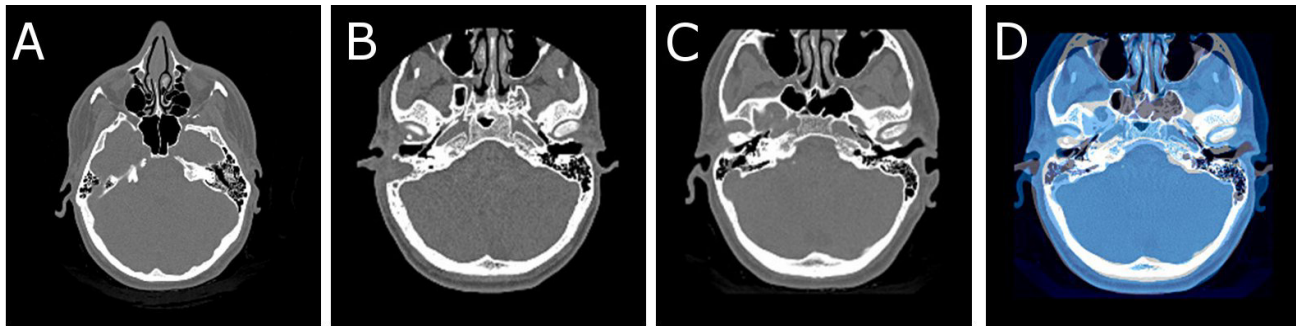


Figure 3 – First step of registration: rigid registration of whole volume – (A) Patient CT scan; (B) atlas; (C) patient scan after registration; (D) correspondence between patient after registration (in blue) and atlas (in grey).

After this first registration has been computed, both the patient CT and atlas images were cropped around the ear canal. The size of this new and smaller image is $44.625 \times 61.25 \times 50 \text{ mm}^3$. This region represents the zone of the skull where the anchors would be implanted for all the PCI patients. It is thus a realistic zone of surgical action. (2) The cropped region of the patient CT and atlas were then rigidly registered again using the same algorithm and similarity measure. This second registration provides a finer alignment of the temporal bone region of each patient to the atlas as shown on Figure 4. (3) Finally, the rigidly aligned cropped regions were registered using a non-rigid registration based on the adaptive bases algorithm¹¹. Figure 5 shows the result of this registration.

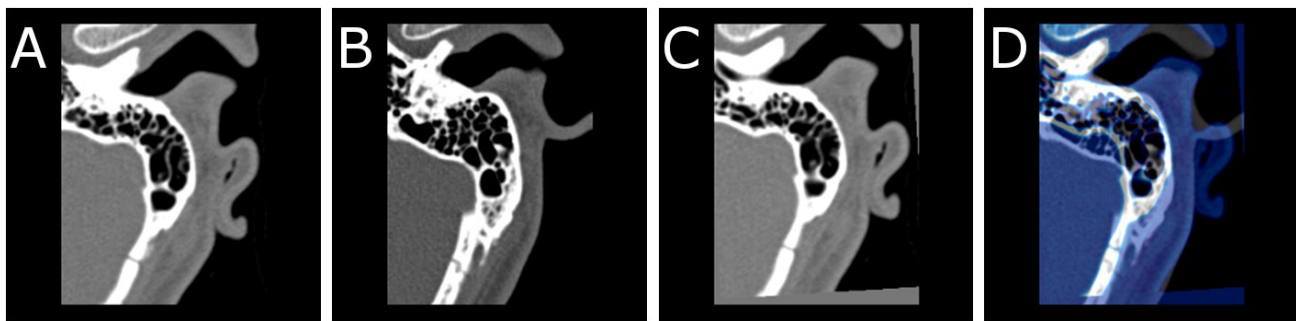


Figure 4 – Second step of registration: rigid registration of subvolumes – (A) Patient CT scan; (B) atlas; (C) patient scan after registration; (D) correspondence between patient after registration (in blue) and atlas (in grey).

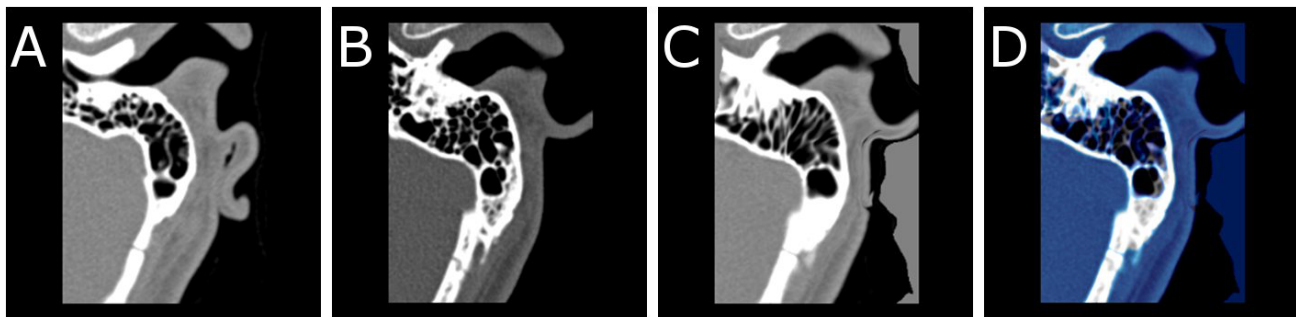


Figure 5 – Final step of registration: non-rigid registration of subvolumes – (A) Patient CT scan; (B) atlas; (C) patient scan after registration; (D) correspondence between patient after registration (in blue) and atlas (in grey).

Figure 6 shows the registration results of five patients. We see that the final result of the registration is visually correct. To further explore the validity of the transformation, we looked closely at the chorda tympani, a small branch of the facial nerve which courses through pneumatized bone. Figure 7 shows that the tubular shape of this structure is preserved and that the chordae are aligned well despite their small size (about 11 mm long and 0.5 mm large).

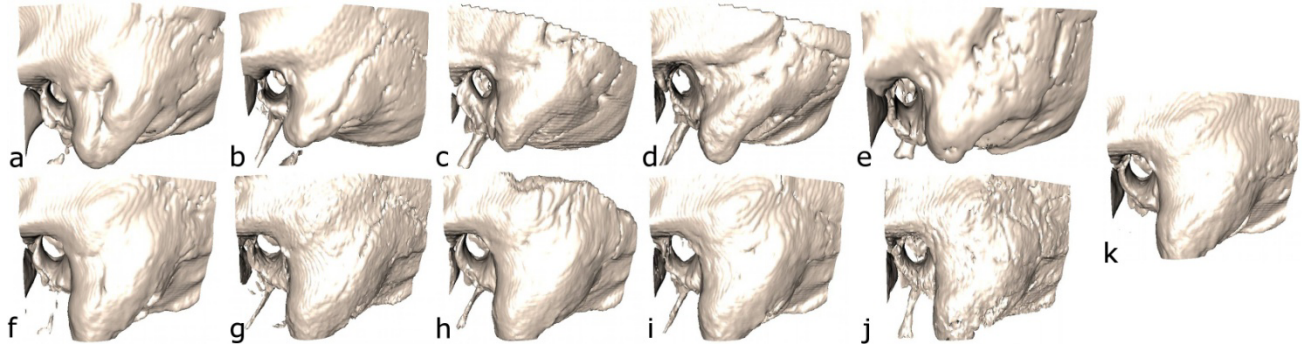


Figure 6 – Example of registration results. (a) to (e): temporal bone from five different patients. (f) to (j) temporal bone of the same patient after registration to the atlas. (k) atlas.

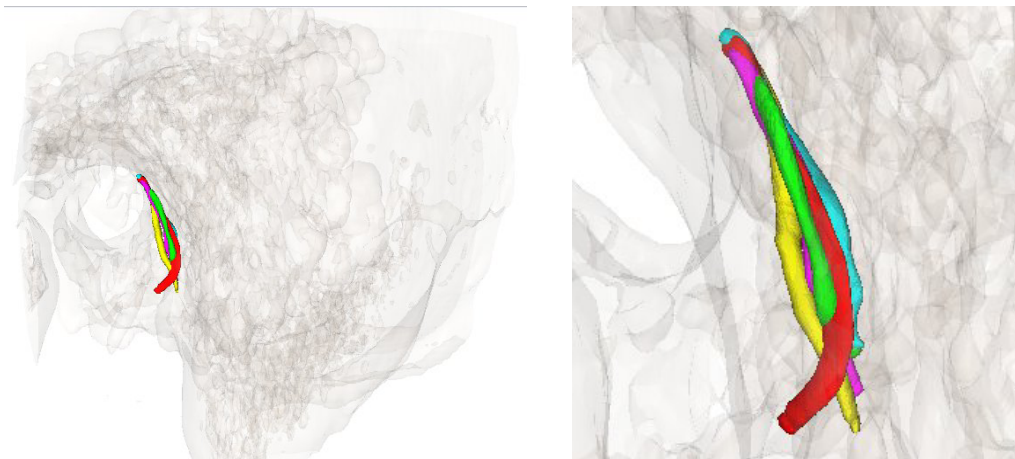


Figure 7 – Visualization of internal structures after the three-step registration. Left: chorda tympani of five patients registered and transformed to the atlas with the temporal bone shown as the transparent structure. Right: magnification of the chordae tympani showing preservation of their shape and good alignment.

2.3. Displacement and differential orientation maps

We were interested in knowing the variability of the temporal bone surface and quantified it using displacement and differential orientation maps among patients. Displacement is measured as the magnitude of the deformation field from the atlas to each of the patient images after the two rigid registrations. The mean and standard deviation of these displacements were then calculated and projected on the mesh of the atlas bone to produce displacement maps. The deformation fields also allow us to pair corresponding points on the surface of the bone.

Another crucial factor in the placement of bone-implanted fiducial anchors is the normal to the surface as the screws of the anchors need to be implanted perpendicularly to the bone to ensure rigid attachment. For each patient and each point in the surface of the cropped region after the two rigid registrations, we computed the outward normal to the surface. The cropped images after the second rigid registration were used because the temporal bones of all patients are locally aligned and the orientation is the same. The normal was also computed for the atlas image. We then computed the angle between the normals for each pair of images (atlas vs. patient). We then again computed the average and standard deviation of these angles to produce differential orientation maps.

2.4. Depth of intracranial structures

In order to quantify the degree with which Macewen's triangle can be considered safe, we need to know how deep from the surface of the skull are the intracranial structures that otological surgeons need to avoid, namely the cochlea, the chorda tympani, the facial nerve, the sigmoid sinus and the carotid artery.

Using the algorithms we have developed for this purpose^{5,6,7}, we segmented those five structures in each of the 25 patients. We were interested in the distance of each structure from the skull as this distance will be the most useful for surgeons as they approach targets following the right-left axis of the head. Using the algorithm developed by Prima et al.¹², we computed the mid-sagittal plane in each of the patients and we defined the right-left axis as the normal to that plane. We then computed the distance between the surface of the skull and each of the five structures along that direction. Figure 8 shows a map of the depth of these structures for a patient. Whenever two structures lied on the path from the skull surface point following the right-left axis, we kept the minimal distance on those maps.

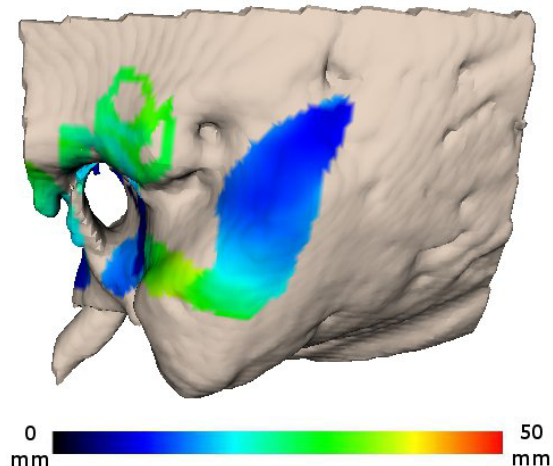


Figure 8 – Depth map of intracranial structure of a patient

Using the registration field defined in the previous sub-section, we registered these maps to the atlas and we then computed the average distance and standard deviation for each skull surface point.

3. RESULTS

3.1. Displacement and differential orientation maps

Figures 9 and 10 show the average and standard deviation of the displacement respectively. The average displacement ranges from 1.36 mm to 5.23 mm while the standard deviation ranges from 0.38 mm to 3.51 mm. Regions usually used to attach the anchors for PCI are labeled in Figure 9 with regions 1 and 3 indicating the suprahelical regions, region 2 indicating the mastoid region, and region 4 indicating the posterior region. The portion of the temporal bone directly above the auditory canal, labeled 1 in Figure 9, exhibits the least displacement, both in average and standard deviation, while the mastoid, labeled 2, is the region of the temporal bone where the displacement is the largest with the largest standard deviation.

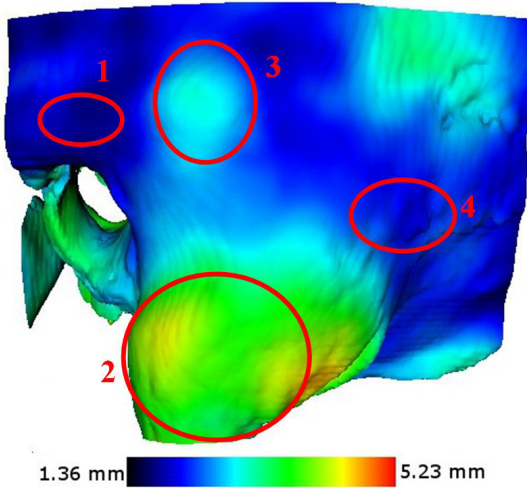


Figure 9 – Average displacement map of the temporal bone

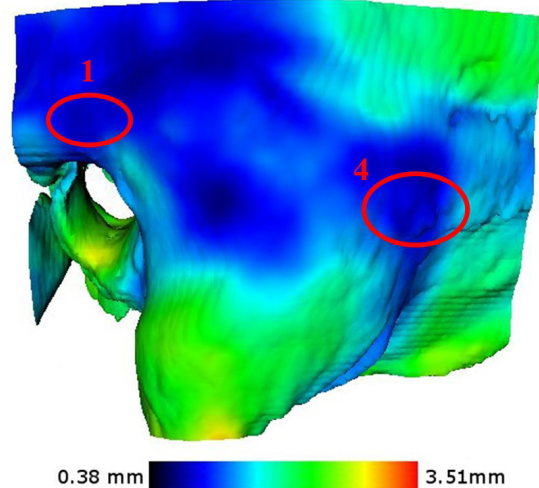


Figure 10 – Standard deviation of displacement map of the temporal bone

The average angle between normals of corresponding points of the surface of the bone ranges from 9.5 to 44.3 degrees while standard deviation ranges from 4.7 to 33.5 degrees. Figure 11 and 12 illustrate those features on the surface of the temporal bone region.

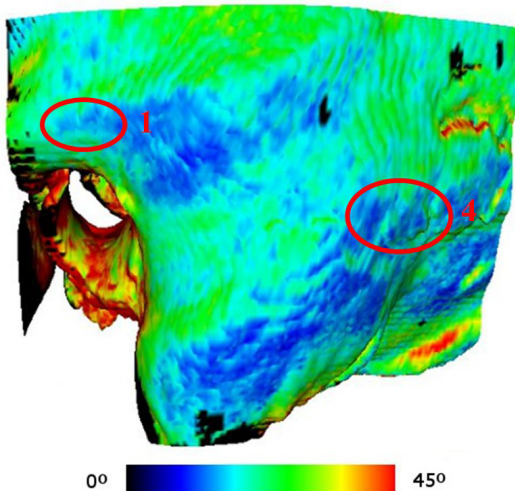


Figure 11 – Mean differential orientation map of the temporal bone

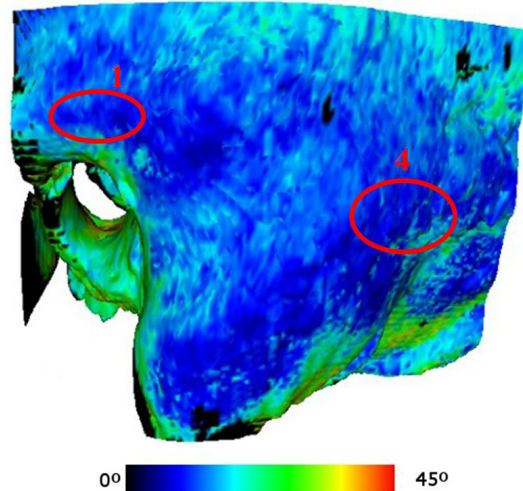


Figure 12 – Standard deviation of differential orientation map of the temporal bone

Based on both the measured features, we can see that regions labeled 1 and 4 exhibit low displacement and low differences in normal orientation. These two zones are very good candidates for bone-implanted, fiducial anchor placement.

Regions labeled 2 and 3 exhibit large displacements. They also correspond to muscle attachments: the sternocleidomastoid muscle for region 2 and the auricularis posterior muscle for region 3. These muscle attachments tend to pull on the bone, hence creating protrusions during osteogenesis.

3.2. Depth of intracranial structures

Figure 13 present the average distance of intracranial structures from the surface of the skull along the right-left axis of the head. In Macewen's triangle region, this distance ranges from 17.8 to 38.3 mm.

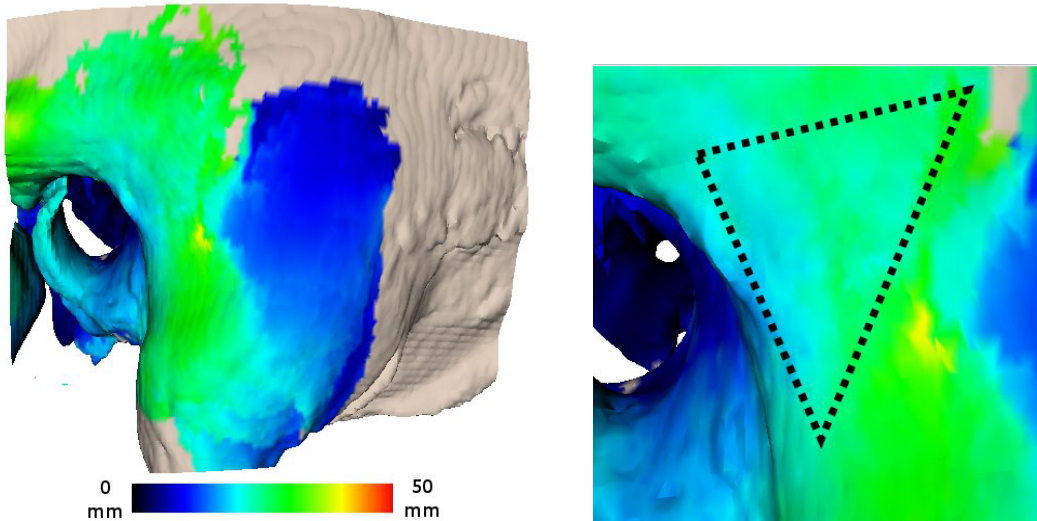


Figure 13 – Average distance of intracranial structures from the surface of the skull– Left: temporal bone – Right: Magnification of Macewen's triangle region (dotted line). Color map from 0 to 50 mm.

Figure 14 provides the standard deviation of the distance from the surface of the skull of those same structures. We observe that this standard deviation is relatively low in Macewen's triangle as it ranges from 0.6 to 7.2 mm. The highest standard deviation is obtained where the depth is between 35 and 38 mm, hence representing less than 20% variation, and only in a small portion of the area..

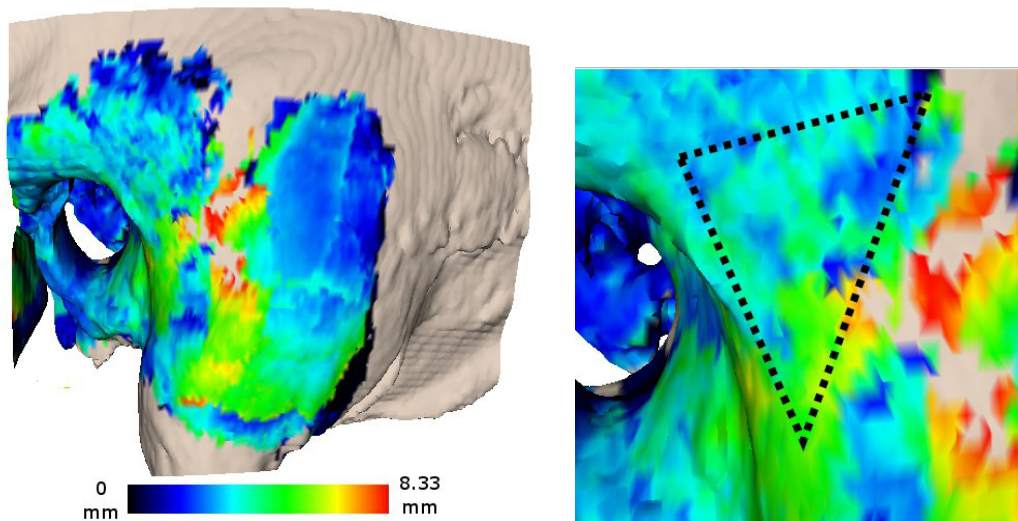


Figure 14 – Standard deviation of the distance of intracranial structures from the surface of the skull - Left: temporal bone – Right: Magnification of Macewen's triangle region (dotted line). Color map from 0 to 8.33 mm.

4. DISCUSSION

To the best of our knowledge, this work reports the first topography study of the temporal bone. Using a combination of two rigid-body and one non-rigid transformation, we were able to compare the temporal bones of twenty five patients and show how they differ. From this comparison, we were then able to define two regions of the skull surface (suprahelical and posterior) exhibiting low variation of displacement and angle that are good candidates for anchor

placement. We were also able to link the highly variable regions to a muscle attachment locations. This work also shows that the mastoid region is highly variable, indicating a difficulty in defining a common location for the third anchor.

Using the atlas space as common space for registration is a potential bias if the atlas is not representative of the population. To tackle that problem, it would be good to reiterate the whole process using an average of the 25 volumes as the new atlas. Moreover, separate atlases may be necessary for specific populations such as children.

We also designed a process to compute the depth of important intracranial structures (chorda tympani, facial nerve, cochlea, sigmoid sinus and carotid artery) from the surface of the skull from the point of view of an otological surgeon. From this measurement, we established that the traditional training, which consider Macewen's triangle to be a safe location to begin intervention, is correct as critical structure lies between 17.8 and 38.3mm deep from that region, hence giving a relatively large margin of safety when beginning to drill.

A limitation of this part of the study is that we did not compute the depth of the brain from the surface of the skull, which infrequently is located inferior to the temporal line (the superior aspect of Macewen's triangle); we are currently addressing this limitation by incorporating the brain into our atlas.

5. CONCLUSION

This study explored the topography of the temporal bone and its implications for otologic surgery. Regarding identification of sites for bone-implanted, fiducial anchor placement, we identified two regions of low inter-patient variability—suprahelical (region 1 in Figure 9) and posterior (region 4 in Figure 9)— which would be good candidates for standard anchor placement. We also discovered that a third standard anchor location may be difficult to find as the traditional third region—mastoid tip (region 2 in Figure 9)—shows high inter-patient variability. We also show that the intracranial structures that otologic surgeries try to avoid are deep enough within Macewen's triangle to confirm that the traditional drilling approach is safe.

ACKNOWLEDGMENTS

This project is supported, in parts, by NIH grants R01DC008408 and R01DC010184 from the National Institute of Deafness and Other Communication Disorders. The content is solely the responsibility of the authors and does not necessarily represent the official views of these institutions.

REFERENCES

- [1] Pickard, B.H., "A Re-Examination of Macewen's Triangle as a Surface Marking for the Mastoid Antrum", *The Journal of Laryngology and otology* 76, 679-682 (1962).
- [2] Macewen W., [Pyogenic and infectious Diseases of the Brain and Spinal Cord], MacLehose & sons, Glasgow, 9 (1893).
- [3] U.S. Food and Drug Administration, "Cochlear implantation", *U.S.F.D.A. PMA no. 840024/S46* - 8/21/95 (1995).
- [4] Labadie, R. F., Balachandran, R., Mitchell, J. E., Noble, J. H., Majdani, O., Haynes, D.S., Bennett, M.L., Dawant, B.M., Fitzpatrick, J.M., "Clinical Validation Study of Percutaneous Cochlear Access using patient-Customized Microstereotactic Frames", *Otology and Neurotology* 31(1), 94-99 (2010).
- [5] Noble, J.H., Majdani, O., Labadie, R.F., Dawant, B.M., Fitzpatrick, J.M "Automatic determination of optimal linear drilling trajectories for cochlea access accounting for drill-positioning error", *International Journal of Medical Robotics and Computer Assist Surgery*, 6(3), 281-290 (2010).
- [6] Noble, J.H., Warren, F. M., Labadie, R.F., Dawant, B.M. "Automatic segmentation of the facial nerve and chorda tympani in CT images using spatially dependent feature values", *Medical Physics* 35(12), 5375-5384 (2008).
- [7] Noble, J.H., Dawant, B.M., Warren, R.M., Majdani, O., Labadie, R.F. "Automatic Identification and 3-D Rendering of Temporal Bone Anatomy," *Otology and Neurotology* 30(4), 436-442 (2009).
- [8] Noble, J.H., Labadie, R.F., Majdani, O., Dawant, B.M., "Automatic segmentation of intra-cochlear anatomy in conventional CT", *IEEE Transactions on Biomedical Engineering* 58(9), 2625-2632 (2011).
- [9] Kratchman, L.B., Blachon, G.S., Withrow, T.J., Balachandran, R., Labadie, R.F., Webster III, R.J. "Design of a Bone-Attached Parallel Robot for Percutaneous Cochlear Implantation", *IEEE Transactions on Biomedical Engineering* 58(10), 2904-2910 (2011).
- [10] Studholme, C., Hill, D. and Hawkes, D., "An overlap invariant entropy measure of 3D medical image alignment", *Pattern Recognition* 32, 71-86 (1999)

- [11] Rohde, G., Aldroubi, A., Dawant, B. "The Adaptive Bases Algorithm for Intensity-Based Nonrigid Image Registration", *IEEE Transactions on Medical Imaging* 22, 1470-1479 (2003)
- [12] Prima, S., Ourselin, S., Ayache, N. "Computation of the Mid-Sagittal Plane in 3D Brain Images", *IEEE Transactions on Medical Imaging* 21(2), 122-138 (2002)